Intermittency of many-particle dispersion in anisotropic magnetohydrodynamic turbulence

J. Pratt[1], A. Busse[2], and W.-C. Müller[3]

[1]Georgia State University, Department of Physics and Astronomy, Atlanta Georgia, 30303, USA
[2]James Watt School of Engineering, University of Glasgow, Glasgow G12 8QQ, United Kingdom
[3]Center for Astronomy and Astrophysics, ER 3-2, TU Berlin, Hardenbergstr. 36, 10623 Berlin, Germany

E-mail: jpratt7@gsu.edu

Abstract. Intermittent deviation from average dispersion curves reveals differences between the dynamics of magnetohydrodynamic turbulence and hydrodynamic turbulence. Turbulent dispersion is typically measured by the average separation of a group of Lagrangian tracer particles from each other as the particles move in a turbulent flow. On average, the particles will increase their separation as time evolves. However, due to the intermittent nature of turbulence, radical deviations from this behavior can be observed when considering individual groups of particles. When the group consists only of two particles, those two particles sometimes can move toward each other for short periods of time, decreasing their separation. When the group consists instead of many particles that are initially densely packed, similar results can be obtained using the convex hull of the group of particles. We examine this intermittency of many-particle dispersion in incompressible isotropic hydrodynamic turbulence, incompressible isotropic magnetohydrodynamic turbulence, and incompressible anisotropic magnetohydrodynamic turbulence. We interpret periods of decreasing separation physically in terms of anisotropic dispersion due to a large-scale static magnetic field, interactions with local magnetic fields and current sheets, and interactions with Alfvénic fluctuations.

1. Introduction

Turbulence affects the trapping and transport of cosmic rays and other energetic particles, magnetic reconnection physics and predictions of space weather, and the mixing of plasma in stellar interiors that is essential to stellar evolution. Diffusion and dispersion are linked to the turbulent conditions of the plasma, and are most naturally and directly studied using the Lagrangian viewpoint.

Magnetohydrodynamic (MHD) turbulence is an area where a statistical analysis using Lagrangian tracer particles has recently begun to be applied [e.g. 5, 6, 13, 10]. These early works have focused on questions of diffusion, dispersion, and transport processes using statistics built from single particles or pairs of particles [for the development and application of these statistics in hydrodynamic turbulence see for example 22, 27, 25, 21]. In this work, we explore how the volume spanned by a larger group (more than 4) of Lagrangian tracer particles can reveal aspects of the anisotropy produced by a macroscopic magnetic field in an electrically conducting fluid or plasma. This kind of anisotropy has been a topic of focus in the field of turbulence for several decades [see 16, 23, 15, 17, 3, 7, 11, 24]. The many-particle Lagrangian statistics developed here provide a new and different piece of the puzzle to provide a more complete description of the anisotropic dynamics of MHD turbulence under the influence of a macroscopic magnetic field.

Dispersion is often measured using pairs of Lagrangian tracer particles. The particles are initialized to a specific distance and their distance is measured at subsequent time steps (see Figure 1). When the average behavior of many such pairs of tracer particles are considered, the average separation of the pairs will increase smoothly in time. However, when a single pair of particles is considered, the

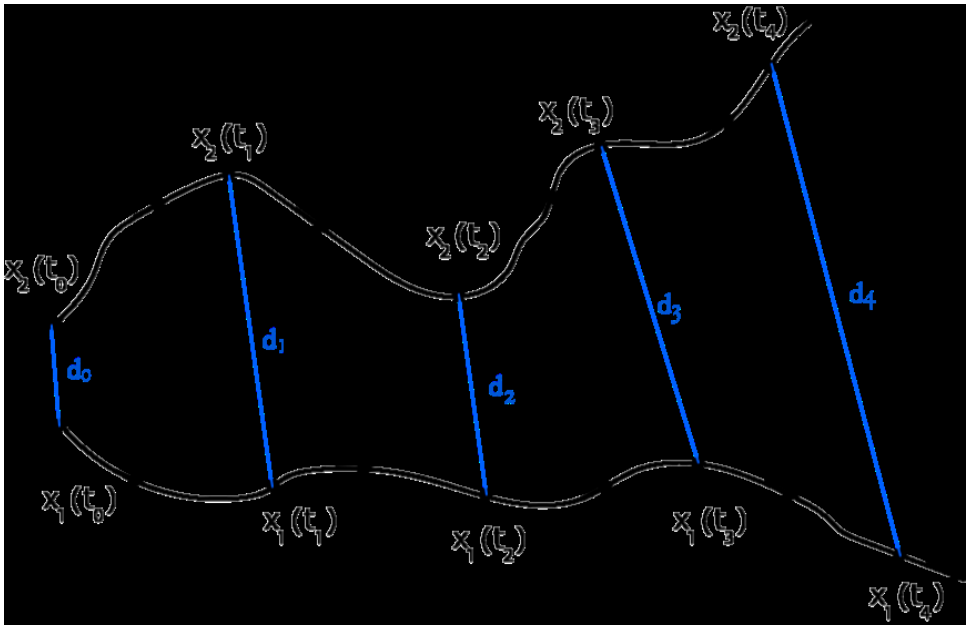

Figure 1. Illustration of the paths of a pair of particles dispersing in a turbulent flow. The position of particle 1 is labeled x_1 and the position of particle 2 is labeled x_2. Distances between the particles are recorded at regular times t_0, t_1, t_2, t_3, t_4; these distances are indicated in blue and labeled d_0, d_1, d_2, d_3, d_4. In this example $d_2 < d_1$ indicating that the distance between a pair of particles can temporarily shrink during turbulent dispersion.

particles may move toward each other at some point, depending on the local conditions of the flow; the separation of any pair of particles will not be smooth and monotonic. If we consider a group of many particles rather than just two, the separation of that group of particles can be similarly erratic. In an anisotropic flow, particles may spread in one direction faster than another direction. Waves, fluctuations, current sheets, or magnetic structures may press some of the particles backward toward the rest of the group. Following the work of Pratt et al. [19], we calculate the convex hull of each group of particles to produce a surface area and volume. We then analyze how the surface areas and volumes of these groups change as the particles disperse. Using the surface area and volume, we can describe the anisotropy of the flow, and reveal new characteristics of anisotropic dispersion.

This work is structured as follows. In Section 2 we describe the physical and numerical models, and the details of the simulations performed. In Section 3 we examine how groups of many particles disperse in these simulations by examining the surface areas and volumes of groups of Lagrangian tracer particles. We compare isotropic and anisotropic systems to provide a new perspective on anisotropic dispersion. In Section 4 we summarize our work and discuss what these results reveal about the processes underlying turbulent dispersion in anisotropic incompressible MHD turbulence.

2. Simulations

We investigate the effect of anisotropy in statistically stationary, forced, homogeneous, incompressible, magnetohydrodynamic turbulence in the presence of a static mean magnetic field[1]. In each direct numerical simulation, we solve the non-dimensional equations for MHD turbulence:

$$\frac{\partial \vec{\omega}}{\partial t} - \nabla \times (\vec{v} \times \vec{\omega} + \vec{j} \times \vec{B}) = \hat{\nu} \nabla^2 \vec{\omega} + \hat{\vec{f}}^{\omega} \ , \tag{1}$$

$$\frac{\partial \vec{B}}{\partial t} - \nabla \times (\vec{v} \times \vec{B}) = \hat{\eta} \nabla^2 \vec{B} + \hat{\vec{f}}^{b} \ , \tag{2}$$

[1] Such a static mean magnetic field has alternatively been referred to an external magnetic field, or a guide-field.

using a pseudospectral method in a rectangular simulation volume with periodic boundary conditions. These equations include the solenoidal velocity field $\vec{v}$, vorticity $\vec{\omega} = \nabla \times \vec{v}$, magnetic field $\vec{B}$, and current $\vec{j} = \nabla \times \vec{B}$. Each of the quantities in eqs. (1) and (2) has been non-dimensionalized using relevant time and length scales, commonly referred to as Alfvénic units. Two dimensionless parameters, $\hat{\nu}$ and $\hat{\eta}$, appear in the equations. They derive from the kinematic viscosity ν and the magnetic diffusivity η. A fixed time-step and a low-storage third-order Runge-Kutta method [26] are used for the time-integration. A static macroscopic magnetic field B_0 is imposed, pointing purely in the positive z-direction.

To maintain the turbulence in steady state, the vorticity and magnetic fields are forced on the largest scales of the simulation volume using a stochastic forcing method (see Eswaran & Pope [9, 8], Busse [4]) that allows the largest scale motions of the system to evolve. This is represented by the forcing terms $\hat{\vec{f}}^{\omega}$ and $\hat{\vec{f}}^{b}$. For simulations HPUFF and APUFF0 the forcing terms are non-zero only for the wave-vector shell $1 \leq |\vec{k}| \leq 2.5$. For simulations APUFF1 and APUFF3, this forcing wave-vector shell is shifted to $2.5 \leq |\vec{k}| \leq 3.5$; this adjustment was made because forcing wave-vectors in the lower k shell in combination with the mean magnetic field was found to lead to a build-up of energy at large scales, significantly changing the energy spectra. Because we simulate MHD turbulence with approximate equipartition of energy, these two forcing constants provide forcing on an identical time-scale for each field. Based on this forcing method, our simulations are consistent with the strong interaction regime of turbulence. Large-scale Alfvén waves are permitted and are observed when stochastic forcing is used.

Table 1. Simulation parameters: magnitude of the static macroscopic magnetic field B_0, the root-mean-square of magnetic fluctuations B_{RMS} averaged over the full simulation time, Kolmogorov time scale τ_η, the large-eddy length scale $\mathrm{L_E}$, and the Kolmogorov microscale η_{kol}. To compensate for the anisotropy in MHD turbulence, the simulation volume is standardly elongated in the z-direction; the elongation of the simulation box is listed in the table for each simulation. The simulation volume has sides of length 2π in the x and y directions. Each simulation is performed on a grid of $N^3 = 1024^3$ and uses 4.5 million particles initialized into droplets.

	B_0	B_{RMS}	$\tau_\eta(10^{-2})$	$\mathrm{L_E}$	η_{kol} (10^{-3})	Re	elongation
HPUFF	–	–	4.20	3.70	3.55	10570	1
APUFF0	0.	1.78	4.89	2.49	3.83	5640	1
APUFF1	1.	1.01	5.03	1.82	3.66	3630	1
APUFF3	3.	1.17	4.82	2.57	3.80	5940	2

Table 1 provides a summary of the fundamental parameters that describe each simulation analyzed in this work. In the table, we record the strength of the macroscopic magnetic field B_0 imposed in the z direction, as well as the root-mean-square of the magnetic fluctuations B_{RMS} in each simulation, averaged over the simulation time. Simulations HPUFF and APUFF0 are isotropic. Simulation APUFF1 has a weak mean magnetic field similar in size to the magnetic fluctuations, and thus a low level of anisotropy. Simulation APUFF3 has a strong mean magnetic field; it is strongly anisotropic and the dynamics are affected by Alfvénic fluctuations. We measure lengths in units of the Kolmogorov microscale $\eta_{\mathrm{kol}} = (\hat{\nu}^3/\epsilon_{\mathrm{v}})^{1/4}$ and time in units of the Kolmogorov time-scale $\tau_\eta = (\hat{\nu}/\epsilon_{\mathrm{v}})^{1/2}$; these are the smallest length and time scales that characterize turbulent flows. Here $\epsilon_{\mathrm{v}} = \hat{\nu}\langle\sum_k k^2\vec{v}^2\rangle$ is the time-averaged rate of kinetic energy dissipation. We select the dissipative parameters and elongation of the simulation box to ensure the resolution criterion ($\mathrm{k_{max}}\eta_{\mathrm{kol}} > 1.5$) is satisfied for adequate spatial resolution [18].

The total number of Lagrangian tracer particles in each simulation is $\mathrm{n_p} \approx 4.5$ million. At each time step the particle velocities are interpolated from the instantaneous Eulerian velocity field using a tricubic polynomial interpolation scheme [see 12]. Like the Eulerian fields, the time integration of the particle positions are calculated using a low-storage third-order Runge-Kutta method.

The positions of the particles are set so that they are initially grouped into spherical "droplets". The position of the particles within the diameter of each droplet is homogeneous and random; the initial position of each droplet within the simulation volume is also homogeneous and random. The droplets are initialized at a time when the turbulent flow is in a statistically stationary steady state.

Lagrangian tracer particles are initialized at two densities within droplets. High-density droplets are created to explore dispersion for smaller droplets; these have a density of 11.5 particles per η_{kol}^3. Low-density droplets are used to explore dispersion for a larger range of sizes; these have a density of approximately 0.006 particles per η_{kol}^3. High-density droplets are initialized into spheres with diameters of $D = 4\eta_{\text{kol}}$, $6\eta_{\text{kol}}$, $8\eta_{\text{kol}}$, and $14\eta_{\text{kol}}$. Low-density droplets are initialized with diameters of $D = 14\eta_{\text{kol}}$, $20\eta_{\text{kol}}$, $26\eta_{\text{kol}}$, $32\eta_{\text{kol}}$, $38\eta_{\text{kol}}$, $44\eta_{\text{kol}}$, $48\eta_{\text{kol}}$, and $64\eta_{\text{kol}}$. In this work we will focus mainly on the two groups with initial diameters $D = 14\eta_{\text{kol}}$, which provide a comparison between low-density and high-density droplets. Other particle groups follow a similar trend to these two groups. For each size of droplets, 200 such droplets are followed for approximately 400 τ_η, a sufficient time that single-particle statistics exhibit a diffusive trend.

The volume, v, and surface area of each droplet are calculated with a convex hull algorithm that uses a Delaunay triangulation of the convex hull vertices at each time step. The convex hull is the smallest convex surface that encloses a set of points; the analogy is to a balloon that surrounds each droplet of Lagrangian tracer particles for the length of the simulation. For a description of the convex hull analysis applied to turbulence, we refer to Pratt et al. [19]. The convex hull calculation is performed using the standard QuickHull algorithm [1, 2], implemented in the function *convhulln* in the package *geometry* publicly available for the R Project for Statistical Computing [14, 20]. The Lagrangian statistics that we produce have been tested for convergence.

3. Results

Like the separation of pairs of particles, the volumes of the different droplets in the simulation grow at different rates. The volumes of the droplets tend to expand smoothly on average, as the particles that define them disperse. However when a single droplet is considered, the growth of its volume may not be smooth, and may sometimes decrease. A comparison between the average volume and a single volume is shown in Figure 2.

The relationship between the surface area and volume of the droplets is central to understanding the physics behind the short periods where the volume shrinks. The local flow can be such that the volume decreases slightly while the surface area of the droplet continues to grow. This can be described by:

$$\text{volume}(t_i) \;<\; \text{volume}(t_{i-1})\ , \tag{3}$$

$$\text{surface area}(t_i) \;>\; \text{surface area}(t_{i-1})\ . \tag{4}$$

This behavior reflects asymmetrical dispersion: the droplet becomes stretched out in one direction, while becoming flatter in another. Visualizations of the droplets as they disperse reinforce that this picture of anisotropic dispersion does often occur. A typical example of the ribbon-like structuring of dispersing droplets in our anisotropic MHD turbulence simulations is shown in Figure 3. As a comparison, particles typically disperse in a cloud-like structure in isotropic hydrodynamic turbulence; a visualization of such an isotropic cloud is provided in Figure 4. Time intervals where conditions (3) and (4) are simultaneously satisfied, we call *ribbon-like dispersion*.

A second scenario is when both surface area and volume decrease at the same time, described by

$$\text{volume}(t_i) \;<\; \text{volume}(t_{i-1})\ , \tag{5}$$

$$\text{surface area}(t_i) \;<\; \text{surface area}(t_{i-1})\ . \tag{6}$$

These conditions correspond to a situation where a subset of the Lagrangian tracer particles in the droplet are being forced back toward the group. The analogy is to a car crash where the front-end is smashed and crumpled into the body of the car. For our droplets, this could happen if the expanding group of particles were confronted with a flow structure of a size similar to or larger than the droplet. We notice that a period where the droplet shrinks is often preceded by a period of

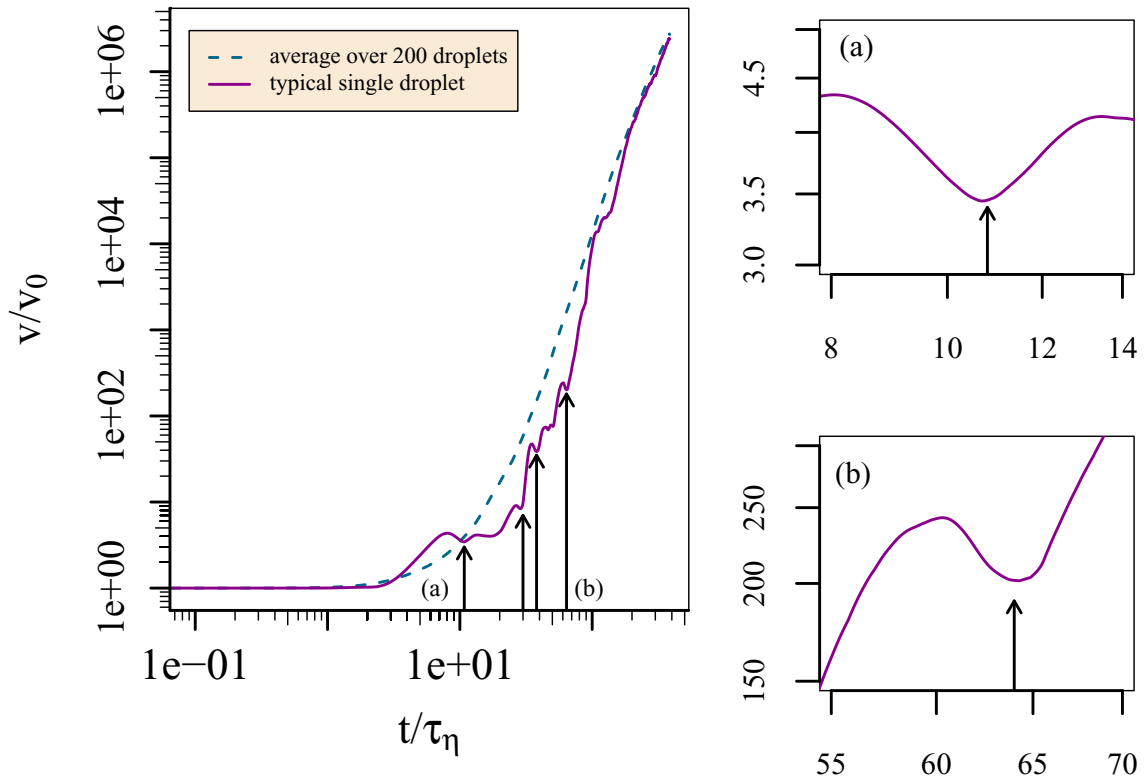

Figure 2. Log-log plot of the evolution of the average over 200 droplets of the volume v divided by the initial volume v_0, compared with a typical single droplet for the simulation APUFF3 described in Table 1. Each of these volumes is defined by the convex hull of a group of 16464 Lagrangian tracer particles. Each of these groups of particles is initialized into a spherical volume of diameter $D = 14\eta_{\text{kol}}$ so that the initial convex hull is a sphere. Visible in this plot are short time-periods where the volume of the droplet decreases; four easily identifiable periods of volume decrease are marked by arrows. Two short periods of volume decrease labeled (a) and (b) are shown in high detail to the right in plots (a) and (b).

ribbon-like dispersion. This suggests that there can be a link between separation of the particles in this extremely anisotropic way, and a flow pattern that causes the droplet to shrink. If a flow structure prevents particles from dispersing unhindered in one direction, the droplet could continue to disperse in other directions. Thus the droplet could disperse in a ribbon-like way for a short period of time, before the influence of the flow structure is large enough to cause the surface area of the droplet to decrease.

To better understand when droplets shrink or show ribbon-like dispersion, we calculate the fraction of droplets that satisfy each of our criteria. For the most anisotropic of our simulations, APUFF3, these fractions are shown in Figure 5. For both ribbon-like dispersion and shrinking, the plot shows a noisy peak between roughly $5\tau_\eta$ and $100\tau_\eta$, a time period that constitutes the inertial range of time scales for the simulation. In Figure 5, the maxima of the peaks are at a fraction of 0.14 (shrinking), and 0.12 (ribbon-like dispersion). For simulations APUFF0 and APUFF1 and the same size droplets, a similar peaked shape is found. In simulation APUFF1, the peaks are at 0.12 (shrinking), and 0.10 (ribbon-like dispersion). In simulation APUFF0, the peaks are at 0.11 (shrinking), and 0.11 (ribbon-like dispersion). In contrast to these MHD dispersion results, for simulation HPUFF and the same size droplets, we find no ribbon-like dispersion after τ_η, and no shrinking at all.

The largest fractions of shrinking or ribbon-like dispersion occur during the period where the

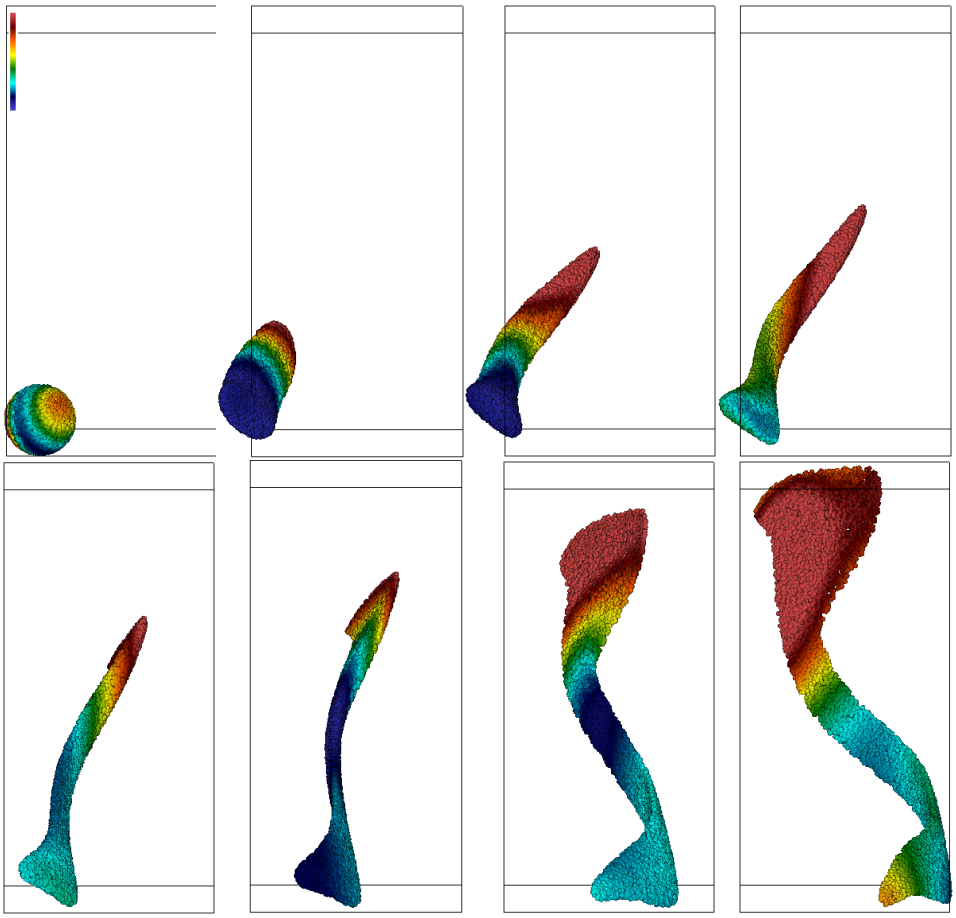

Figure 3. Dispersion of a single droplet consisting of 16464 Lagrangian tracer particles in simulation APUFF3 over $12\tau_\eta$, shown from a 3D perspective. The particles are initialized into a sphere of diameter $14\eta_{\text{kol}}$. Each panel has an identical color scale, and each particle is colored by the kinetic energy of the flow that it experiences.

volume grows to 2-3 hundred times its original size on average (see panel (b) of Figure 5). After the noisy peak, these fractions both reduce even as the droplet volume grows. This points to a complex relation between the density of Lagrangian tracer particles within the droplet, the flow dynamics, and the probability that a droplet will shrink.

To further probe this dependence on particle density, we compare high-density and low-density droplets in our simulations. In Figure 6 this is illustrated through a probability distribution function (PDF) of the time derivative of volume. So that droplets in different simulations and droplets that have different volume can be compared, this time derivative is normalized by τ_η/v and is nondimensional. The PDF is constructed over the time period $20\tau_\eta < t < 80\tau_\eta$ for each simulation. For simulation HPUFF, the normalized time derivative of volume ranges between $(-0.6, 1.6)$ for low-density droplets; for high-density droplets this derivative no longer takes negative values, and has a range of $(0.04, 0.51)$. A higher density of Lagrangian tracer particles better resolves these small changes in volume, and can eliminate them for isotropic hydrodynamic turbulence. For simulation APUFF3, the normalized time derivative of volume ranges between $(-4.6, 6.0)$ for low-density droplets; this range is reduced to $(-0.38, 0.73)$ for high-density droplets. The mean indicated by the distributions in each of our simulations is approximately 0.10, for both low-density and high-density droplets. The range of the normalized time derivative of volume is asymmetrical about this mean for all of our simulations, but the high-density droplets in APUFF3 maintain a less asymmetrical range than the low-density droplets in HPUFF. Instances when the volume shrinks are not eliminated, but are smaller, when considered using a higher resolution of Lagrangian tracer particles in MHD turbulence.

We cannot exclude the possibility that this negative volume change might be entirely eliminated for even higher particle densities. However this may point to the need for different resolution requirements in MHD turbulence than hydrodynamic turbulence. It also indicates that the dynamics of dispersion in MHD turbulence are different from hydrodynamic turbulence.

4. Summary and Discussion

We examine many-particle dispersion in incompressible isotropic hydrodynamic turbulence, isotropic magnetohydrodynamic turbulence, and anisotropic magnetohydrodynamic turbulence. Using a surface area and volume obtained from the convex hull of droplets consisting of many Lagrangian tracer particles, we quantify ribbon-like dispersion, as well as periods where the group of tracer particles moves toward each other rather than separating.

If a low density of Lagrangian tracer particles is used, some amount of both ribbon-like dispersion and shrinking can be attributed to a lack of resolution of the droplet by the particles. When we increase this density by a factor of 2000, the small amounts of shrinking and ribbon-like dispersion calculated in our isotropic hydrodynamic turbulence simulation vanish. However our MHD simulations continue to have both ribbon-like dispersion and shrinking droplets at this high density; the increase

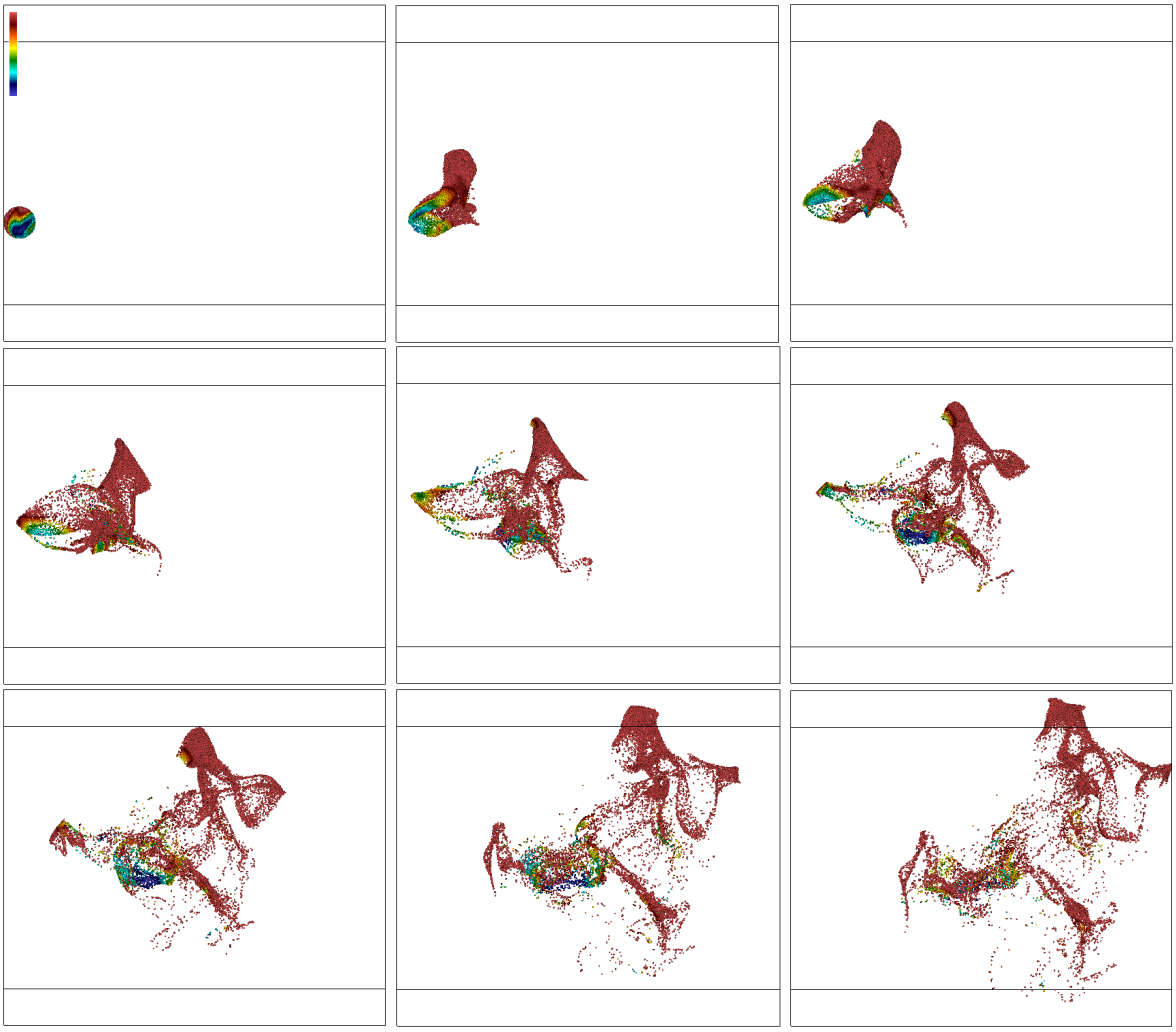

Figure 4. Dispersion of a single droplet consisting of 16464 Lagrangian tracer particles in simulation HPUFF3 over $14\tau_\eta$, shown from a 3D perspective. The particles are initialized into a sphere of diameter $14\eta_{\mathrm{kol}}$. Each panel has an identical color scale, and each particle is colored by the kinetic energy of the flow that it experiences.

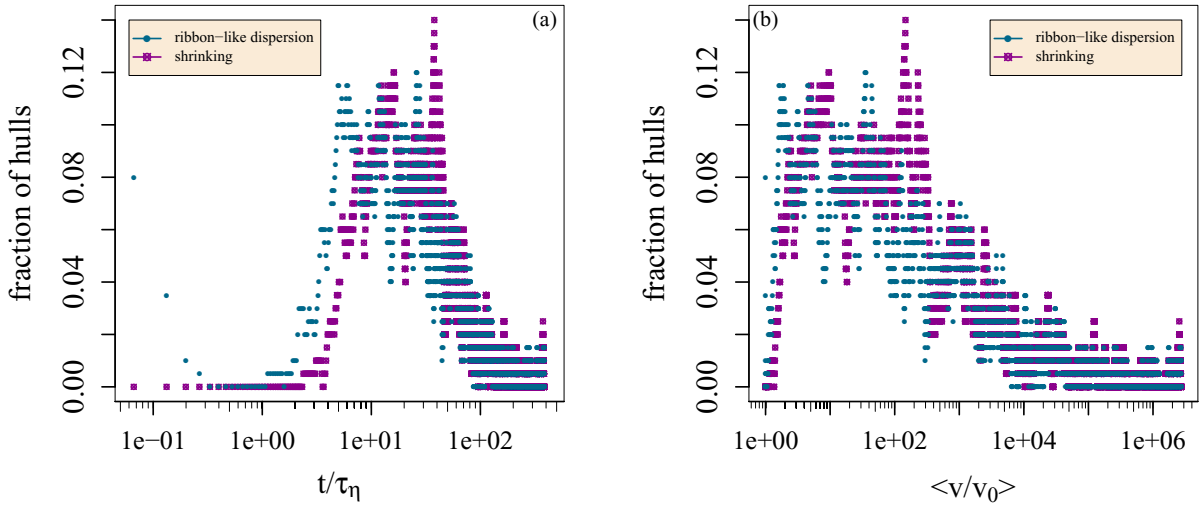

Figure 5. Time evolution of the fraction of droplets shrinking (satisfying eqs. (5) and (6)) and exhibiting ribbon-like dispersion (satisfying eqs. (3) and (4)) in simulation APUFF3. (a) Fraction of droplets vs time in units of the Kolmogorov time scale, and (b) fraction of droplets vs average volume divided by initial volume v/v_0 for the full simulation time. Two hundred droplets consisting of 16464 tracer particles (corresponding to our high-density droplet group) are considered. The initial diameter of the spherical droplet is $D = 14\eta_{\text{kol}}$.

in density appears to result in a lower calculated negative change in the volume and surface area of the droplets. At their peak, more than 10% of hulls in MHD simulations experience either ribbon-like

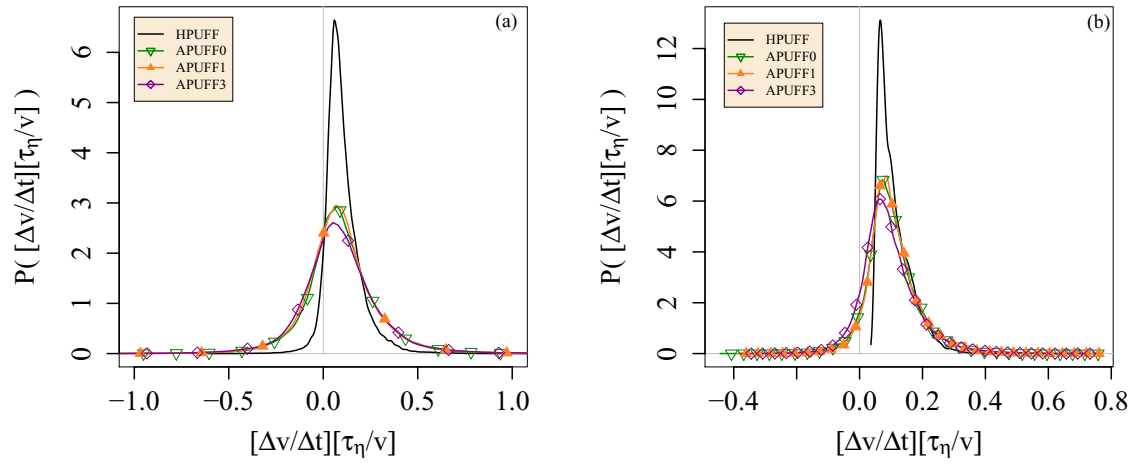

Figure 6. PDF of the nondimensional time derivative of volume divided for the simulations described in Table 1 over the period $20\tau_\eta < t < 80\tau_\eta$. Lagrangian tracer particles are initialized into spherical droplets with diameters $D = 14\eta_{\text{kol}}$. Each PDF is constructed from 200 such droplets. Droplets consist of (a) 8 tracer particles, and (b) 16464 tracer particles. For the low-density droplets, minimum values of this derivative are -0.6 (HPUFF), -3.0 (APUFF0), -5.1 (APUFF1), and -4.6 (APUFF3). For the high-density droplets, minimum values of this derivative are 0.04 (HPUFF), -0.44 (APUFF0), -0.40 (APUFF1), and -0.38 (APUFF3).

dispersion or shrinking. Thus these dispersive behaviors are comparatively rare, but a significant and persistent aspect of many-particle dispersion. Both of these dispersive behaviors occur intermittently in time and last for short periods of time. When the PDF of normalized volume change is examined, these dispersive behaviors define the wing of the distribution.

Periods of ribbon-like dispersion or shrinking appear persistently in all of our MHD simulations, indicating that at a fundamental level, interactions with local magnetic fields and current sheets contribute to these dispersive behaviors. These intermittent dispersive behaviors become more frequent in the presence of the strong mean magnetic field in simulation APUFF3. This is likely a consequence of the interaction with the current sheets that align with the mean magnetic field and the strong Alfvénic fluctuations present in the simulation.

Acknowledgments
This material is based upon work supported by the National Science Foundation under Grant No. 1907876. Simulations were performed on the Konrad and Gottfried computer systems of the Norddeutsche Verbund zur Förderung des Hoch- und Höchstleistungsrechnens (HLRN) by the project bep00051 "Lagrangian studies of incompressible turbulence in plasmas".

References

[1] Barber, C. B., Dobkin, D. P., & Huhdanpaa, H. 1996, ACM Transactions on Mathematical Software, 22, 469

[2] Barber, C. B., Dobkin, D. P., & Huhdanpaa, H. 2013, Astrophysics Source Code Library, record ascl:1304.016

[3] Boldyrev, S. 2006, Phys. Rev. Lett., 96, 115002

[4] Busse, A. 2009, PhD thesis, Universität Bayreuth

[5] Busse, A., & Müller, W.-C. 2008, Astron. Nachr., 329, 714

[6] Busse, A., Müller, W.-C., Homann, H., & Grauer, R. 2007, Phys. Plasmas, 14, 122303

[7] Chandran, B. D. 2008, Astrophys. J., 685, 646

[8] Eswaran, V., & Pope, S. 1988, Phy. Fluids, 31, 506

[9] Eswaran, V., & Pope, S. B. 1988, Computers & Fluids, 16, 257

[10] Eyink, G. L., & Benveniste, D. 2013, Phys. Rev. E, 88, 041001

[11] Haugen, N. E. L., & Brandenburg, A. 2004, Phys. Rev. E, 70, 036408

[12] Homann, H., Dreher, J., & Grauer, R. 2007, Comput. Phys. Commun., 177, 560

[13] Homann, H., Ponty, Y., Krstulovic, G., & Grauer, R. 2013, arXiv preprint arXiv:1309.7975

[14] Ihaka, R., & Gentleman, R. 1996, J Comput. Graph. Stat., 5, 299

[15] Matthaeus, W. H., Ghosh, S., Oughton, S., & Roberts, D. A. 1996, J. Geophys. Res., 101, 7619

[16] Montgomery, D., & Turner, L. 1981, Phys. Fluids, 24, 825

[17] Müller, W.-C., Biskamp, D., & Grappin, R. 2003, Phys. Rev. E, 67, 066302

[18] Pope, S. B. 2000, Turbulent flows (Cambridge University Press)

[19] Pratt, J., Busse, A., Müller, W., Watkins, N., & Chapman, S. C. 2017, New Journal of Physics, 19, 065006

[20] R Core Team. 2014, R: A Language and Environment for Statistical Computing, R Foundation for Statistical Computing, Vienna, Austria

[21] Salazar, J. P., & Collins, L. R. 2009, Annu. Rev. Fluid Mech., 41, 405

[22] Sawford, B. 2001, Annu. Rev. Fluid Mech, 33, 289

[23] Shebalin, J. V., Matthaeus, W. H., & Montgomery, D. 1982, PhD thesis, Cambridge Univ Press

[24] Sujovolsky, N. E., & Mininni, P. D. 2016, Phys. Rev. Fluids, 1, 054407

[25] Toschi, F., & Bodenschatz, E. 2009, Annu. Rev. Fluid Mech., 41, 375

[26] Williamson, J. H. 1980, J. Comput. Phys., 35, 48

[27] Yeung, P. 2002, Annu. Rev. Fluid Mech., 34, 115